A Strategy for Robust Precision Control of an Endbody being Towed by an Orbiting UAV

Mariann Merz *, Tor Arne Johansen†

Center for Autonomous Marine Operations and Systems

Norwegian University of Science and Technology, Trondheim, 7491, Norway

This paper presents a strategy for end-body positioning maneuvers using a towed cable-body system where a fixed wing Unmanned Aerial Vehicle (UAV) is stabilized in a circular orbit. High precision maneuvers such as object pickup/dropoff are typically performed by rotorcraft UAVs, but a successful fixed-wing concept would greatly increase the possible range for this type of operation and enable missions into more remote locations. Circularly towed cable-body systems have been shown capable, both analytically and experimentally, of maintaining stable configurations with the towed endbody maintaining a small motion respective to a point on the ground. However, no known efforts consider small to medium scale UAV operations for object pickup/dropoff/manipulation. A viable concept must be able to perform well when subjected to likely disturbances such as wind that causes the center of orbit for the towed endbody to be offset downwind of the UAV orbit. It is a primary goal of this paper to develop robust UAV path control that is able to stabilize the towed endmass in the presence of both moderate disturbances and modelling uncertainties. An optimized disturbance-free planned path that considers the UAV performance constraints is computed offline for the desired UAV towed system. A nonlinear sliding mode controller is developed to provide robust path control. To compensate for persistent winds or disturbances, the optimized disturbance-free orbit is inclined vertically to achieve an even tug on the towcable (i.e stabilize the measured cable tension force).

I. Introduction

The vast and inaccessible maritime arctic regions are currently the subject of several research initiatives both for the purposes of resource exploitation and for environmental monitoring. The Norwegian University of Science and Technology is researching technologies to support this development, including the capability of deploying fixed-wing UAVs for various long-range missions. Circular towing is looked into as a way to increase the range of possible missions, by adding the possibility of maneuvers such as low-altitude surveillance at speeds lower than the minimum UAV speed, facilitating high-precision, gentle object placement of instruments/equipment that are sensitive to g-forces, and the possibility of manipulating or retrieving small objects. While it has been shown that an optimally configured steady-state circular towing scenario in the absence of wind and disturbances yields an endbody that is stabilized in a low speed, small radius orbit relative to a point on the ground, the challenging operating conditions in the arctic and maritime environments demands a design that is fairly robust to moderate wind levels and also to some degree to small variations in wind magnitude and direction.

A review of key publications related to the general modelling and dynamics of circularly towed aerial systems is provided in Ref. 1. Specifically relevant for the present work are publications from the TACAMO project that describes challenges and lessons learned from a circularly towed long-trailing wire antenna that has been operated by the U.S. Air Force on a regular basis for several decades. Borst, Greisz and Quynn[2] describes the development of a fuzzy logic control algorithm for suppressing wind induced altitude "yoyo" oscillations of the long trailing antenna. Brushwood, Olson and Smyth[3] state that flight testing with the automated Anti-YoYo (AYY) function consistently decreased the peak-to-peak tension oscillations

*PhD Candidate, Department of Engineering Cybernetics, mariann.merz@itk.ntnu.no

†Professor, Department of Engineering Cybernetics.

of the towed antenna and that the vertical oscillations generally decreased by seventy percent. While the TACAMO work is focused on maximizing the verticality of the towcable/antenna rather than minimizing the motion of the towed endbody, this work gave reason to believe that the towcable tension could be a useful feedback parameter to a controller aimed at stabilizing the position of the endbody in the presence of winds and other disturbances. A U.S. Air Force research report from 1972[4] studying the yoyo phenomenon concludes that controlling to a nonconstant altitude orbit is the favored method (in terms of performance) to eliminate or minimize the altitude oscillations caused by winds. Several later studies confirm these results.[5,6] The suveyed literature adopt a number of different approaches to control the position of the towed endmass. Active control of the towed body is discussed in Ref. 7 and Williams study the effect of controlling the cable length.[6] Finally, the control of the cable endmass through manipulation of the towing vehicle motion is considered by many, including in Ref. 2 and Ref. 5. This last approach is popular, and is also the subject of the present study, as it does not require design of additional mechanisms. For a UAV towed system the allowable weight of the towed body is very low, hence a complex control scheme for the towed body is not feasable. The current research plan involves first to study the achievable performance resulting from control of the UAV only, then to consider possible strategies for towed object manipulation as an additional measure to arrive at the desired performance.

The objective of this paper is to develop a scheme to derive a close to optimal path for the towing UAV that minimizes the towed endbody motion in the presence of steady disturbances and to develop a Sliding Mode Controller (SMC) to provide robust path tracking. SMC is a nonlinear technique that provides robust control with respect to matched uncertainties and disturbances which is viewed as a key characteristics in order to succeed with a useful circularly towed concept involving a UAV.

II. Modelling of Physical System

In this section the model used to represent the physical UAV towed system is described. The reference coordinate system and system geometry used for the mathematical modelling is illustrated in Fig 1 and is further described in the next subsection. The system is made up of three distinct components, the towing UAV, the towcable and the towed endmass, each described in the subsections following. Finally, the last subsection provides the system properties that have been assumed for the numerical analysis performed in the last section of this paper.

A. System Geometries

The right-handed Cartesian coordinate system XYZ with origin O and unit vectors **I**, **J** and **K** is the inertial reference frame which is located on the ground level. For the purposes of this paper, we will assume that O coincides with the center of the desired orbit for the UAV, while recognizing that the exact location of the orbit will have to be determined based on the location of the desired dropoff/pickup point on the ground and the predicted towcable shape. The angle θ represents the angle between the horizontal projection of the UAV position vector relative to the X-axis. To model the UAV dynamics we will also need to transform a vector from the inertial coordinate system to the UAV body-fixed coordinate system and vice-versa. The inertial reference frame can be related to the UAV body-fixed reference frame with unit vectors $\mathbf{b_1}$, $\mathbf{b_2}$ and $\mathbf{b_3}$ using a

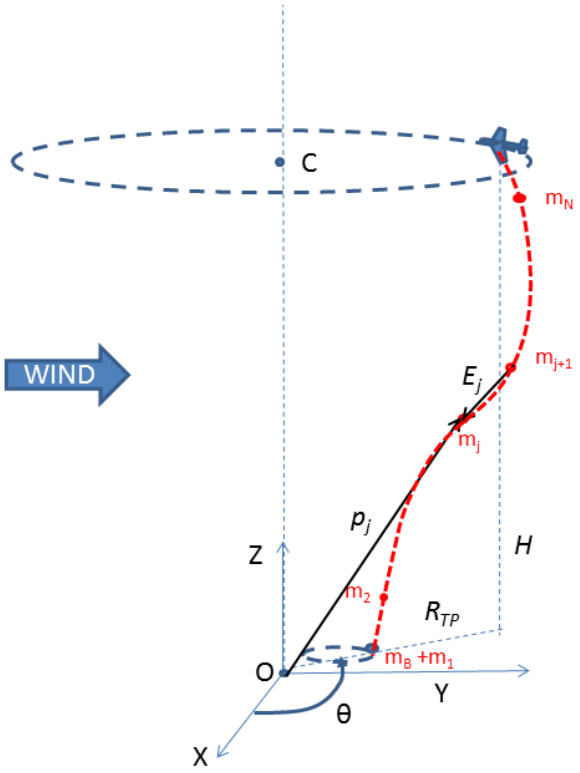

Figure 1. UAV Towed System Geometries.

yaw (ψ), flight path (γ), and bank (ϕ) Euler angle rotation sequence.

$$\mathbf{R_T} = \begin{bmatrix} \cos\phi\cos\psi - \sin\phi\sin\gamma\sin\psi & \cos\phi\sin\psi + \sin\phi\sin\gamma\cos\psi & -\sin\phi\cos\gamma \\ -\cos\gamma\sin\psi & \cos\gamma\cos\psi & \sin\gamma \\ \sin\phi\cos\psi + \cos\phi\sin\gamma\sin\psi & \sin\phi\sin\psi - \cos\phi\sin\gamma\cos\psi & \cos\phi\cos\gamma \end{bmatrix} \tag{1}$$

Conversion from body axis coordinates to inertial coordinates is achieved by use of the transpose of the rotation matrix (R_T).

B. Towing UAV Model

The low mass and operating speeds associated with a UAV towing vehicle makes UAV towed systems particularly sensitive to the loads generated by the towed cable and endmass and also to atmospheric disturbances such as winds. While operation of the UAV system will likely be impossible in strong winds, it should be designed to handle low to moderate winds in order to provide operators with a useful service. To ensure that the limitations of the UAV performance is taken into account it is necessary to use simplified point mass equations of motion for the simulation work rather than just specifying the desired UAV/towpoint motion. V_{UAV} is the airspeed magnitude of the UAV as it would be measured by onboard instruments, so relative to the airmass (i.e V_{UAV} would be higher than the groundspeed when flying into the wind). Since the circular towing maneuver will require operations close to the minimum speed of the UAV,[1] controlling to a constant V_{UAV} provides some measure of safety (protection against stall) since this speed directly impacts the aerodynamic performance.

From kinematics we have that the inertial velocity of the UAV can be expressed as follows:

$$\dot{p}_{UAV_X} = -V_{UAV}\sin\psi\cos\gamma + w_x \tag{2}$$
$$\dot{p}_{UAV_Y} = V_{UAV}\cos\psi\cos\gamma + w_y \tag{3}$$
$$\dot{p}_{UAV_Z} = V_{UAV}\sin\gamma + w_z \tag{4}$$

The above equations can be written in vector form as:

$$\mathbf{\dot{p}_{UAV}} = \mathbf{V_R} + \mathbf{w} \tag{5}$$

$\mathbf{V_R}$ and $\mathbf{w}$ represents the velocity vector of the UAV with respect to the surrounding air and the known steady wind vector respectively, both expressed relative to the inertial frame. The inertial acceleration can be expressed in terms of body axes ($\mathbf{b_1}, \mathbf{b_2}, \mathbf{b_3}$) taking the Coriolis effects into account:

$$\mathbf{\ddot{p}_{UAV}} = -V_{UAV}\left(\dot{\gamma}\sin\phi + \dot{\psi}\cos\gamma\cos\phi\right)\mathbf{b_1} + \dot{V}_{UAV}\mathbf{b_2} + V_{UAV}\left(\dot{\gamma}\cos\phi - \dot{\psi}\cos\gamma\sin\phi\right)\mathbf{b_3} \tag{6}$$

The summation of forces acting on the aircraft are:

$$\begin{aligned}\sum \mathbf{F}_{UAV} &= (Mg\sin\phi\cos\gamma + F_{Cb_1})\mathbf{b_1} + (T_{UAV} - D - Mg\sin\gamma + F_{Cb_2})\mathbf{b_2} \\ &+ (L - Mg\cos\gamma\cos\phi + F_{Cb_3})\mathbf{b_3}\end{aligned} \tag{7}$$

M denotes the UAV mass and T_{UAV}, D, L and $\mathbf{F_C}$ represents the thrust force, drag force, lift force and towcable force acting on the UAV. Now we can get expressions for the dynamics by applying Newton's Second Law.

$$-V_{UAV}\left(\dot{\gamma}\sin\phi + \dot{\psi}\cos\gamma\cos\phi\right) = g\cos\gamma\sin\phi + \frac{F_{Cb_2}}{M} \tag{8}$$
$$\dot{V}_{UAV} = \frac{T_{UAV}}{M} - \frac{D}{M} - g\sin\gamma + \frac{F_{Cb_1}}{M} \tag{9}$$
$$V_{UAV}\left(\dot{\gamma}\cos\phi - \dot{\psi}\cos\gamma\sin\phi\right) = \frac{L}{M} - g\cos\gamma\cos\phi + \frac{F_{Cb_3}}{M} \tag{10}$$

The first and third equations can be solved for $\dot{\gamma}$ by multiplying by $\sin\phi$ and $\cos\phi$ respectively and subtracting the resulting expressions. Similarly they can be solved for $\dot{\phi}$ by multiplying the first equation by $\cos\phi$ and

the third equation by $\sin\phi$ and adding the expressions. The dynamic UAV equations can then be written as:

$$\dot{\gamma} = \frac{L\cos\phi}{MV_{UAV}} - \frac{g\cos\gamma}{V_{UAV}} + \frac{F_{Cb_3}\cos\phi - F_{Cb_2}\sin\phi}{MV_{UAV}} \tag{11}$$

$$\dot{V}_{UAV} = \frac{T_{UAV}}{M} - \frac{D}{M} - g\sin\gamma + \frac{F_{Cb_1}}{M} \tag{12}$$

$$\dot{\psi} = -\frac{L\sin\phi}{MV_{UAV}\cos\gamma} - \frac{(F_{Cb_3}\sin\phi + F_{Cb_2}\cos\phi)}{MV_{UAV}\cos\gamma} \tag{13}$$

The lift and drag forces are assumed to have the following form:

$$L = qC_{L_{UAV}}S = q[C_{L\alpha}(\alpha - \alpha_0)]S \tag{14}$$

$$D = q\left(C_{Dp} + \frac{{C_{L_{UAV}}}^2}{\pi e \mathcal{AR}}\right)S \tag{15}$$

where q is dynamic pressure, $C_{L_{UAV}}$ is the overall lift coefficient, $C_{L\alpha}$ is the lift coefficient for the particular angle of attack, C_{Dp} is the zero-lift parasitic drag coefficient S is the wing surface area, e is the Oswald coefficient and $\mathcal{AR}$ is the wing aspect ratio. The force applied to the UAV by the towed system ($\mathbf{F_C}$) is opposite that computed for of the top element of the cable ($\mathbf{T_N}$), hence the tension force in the UAV body axes can be computed from:

$$\mathbf{F_C} = -\mathbf{R_T}\mathbf{T_N} \tag{16}$$

C. Towcable Model

Early research efforts related to the dynamics of towed systems revealed that for scenarios involving a long tow-cable and/or a fairly light weight towed body, the cable dynamics is so dominant that it is neccessary to treat the cable as a complete aerodynamic body with properties such as shape, size, mass distribution and elasticity.[8] The equations of motion for the towing cable are approximated by replacing the continuous cable with a set of N mass points that are connected with massless, elastic thin rods (to model stretching of the cable). The point mass associated with each cable element is numbered from 1 at the cable end-point through N at the tow-aircraft attachment point. A simplification is made to lump all the external forces acting on each element at the point mass (node), which effectively decouples the acceleration terms between nodes and thereby eliminates the inertial coupling between elements that complicates a standard Finite Element Model (FEM). The simplification allows the motion of each node to be uniquely determined at each time step. The degrees of freedom at each node are coupled to the neighboring nodes through the tension and strain which acts along the connections. For the purposes of this study, it is assumed that the unstrained cable segment lengths (l) between the different point-masses are equal and also that the required length of the cable is equivalent to the total available length (Lc). This type of cable model is known as a discrete Lumped Parameter Model (LPM). Newton's second law applied to the jth point-mass along the towed cable gives:

$$\mathbf{F_j} = m_j\mathbf{a_j}, \quad j = 2, 3, ..., N \tag{17}$$

Similarly, for last cable element with the attached endbody, we have

$$\mathbf{F_B} + \mathbf{F_1} = (m_B + m_1)\mathbf{a_1} \tag{18}$$

Where $\mathbf{F_B}$ and m_B are the forces and the mass of the towed body respectively. The mass of each point mass is

$$m_j = \rho_c l\frac{\pi d^2}{4}, \quad j = 1, 2, 3, ..., N \tag{19}$$

In the above equation, ρ_c is the material density, and d is the diameter of the cable. The inertial acceleration of each point-mass can be obtained from the second derivative of its position relative to the inertial frame. The position vector ($\mathbf{p_j}$) and the velocity vector ($\mathbf{v_j}$) of the jth point mass is given by:

$$\mathbf{p_j} = x_j\mathbf{I} + y_j\mathbf{J} + z_j\mathbf{K} \tag{20}$$

$$\mathbf{v_j} = \dot{x}_j\mathbf{I} + \dot{y}_j\mathbf{J} + \dot{z}_j\mathbf{K} \tag{21}$$

A vector representing each cable element can be computed from the positions of the point masses:

$$\mathbf{E_j} = (x_j - x_{j+1})\mathbf{I} + (y_j - y_{j+1})\mathbf{J} + (z_j - z_{j+1})\mathbf{K} \tag{22}$$

The magnitude of this vector represents the stretched length of the element, and the orientation of the element can be represented by the unit vector obtained from dividing $\mathbf{E_j}$ by it's magnitude. The accelerations of each lumped mass can be obtained from Newton's second law:

$$\mathbf{a_j} = \ddot{\mathbf{p}}_\mathbf{j} = \frac{\sum \mathbf{F_j}}{m_j} \tag{23}$$

The relevant forces to include in the analysis are the external forces due to the aerodynamic effects ($\mathbf{F_{a_j}}$) and gravity ($\mathbf{F_{g_j}}$) acting on the point masses as well as the internal tension force ($\mathbf{T_j}$) acting between each of the neigbouring point masses. Fig. 2 illustrates the forces acting on the jth point mass along the tow-cable. The forces used are:

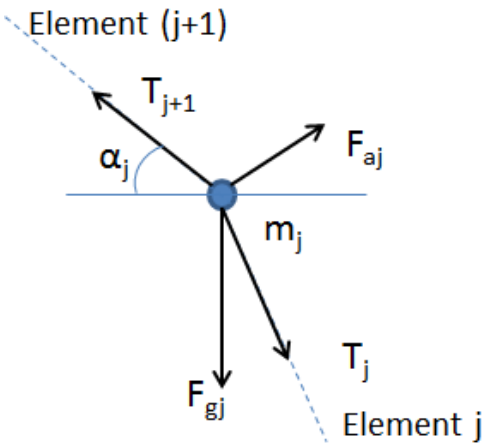

Figure 2. The Forces Acting on a Point Mass

$$\mathbf{F_{g_j}} = m_j g\mathbf{K} \tag{24}$$

$$\mathbf{F_{a_j}} = \frac{1}{2}\rho_a |v_{R_j}|^2 ld(C_{d_j}\mathbf{e_{D_j}} + C_{L_j}\mathbf{e_{L_j}}) \tag{25}$$

$$\mathbf{T_j} = \frac{EA(|\mathbf{E_j}| - l)}{l} \cdot \frac{\mathbf{E_j}}{|\mathbf{E_j}|} \tag{26}$$

E is the modulus of elasticity of the towcable and A is the cross-sectional area of the towcable. The aerodynamic pressure force coefficients are taken as:

$$C_{D_j} = C_f + C_{D_{basic}}(\sin^3 \alpha_j) \tag{27}$$

$$C_{L_j} = C_{D_{basic}}(\sin^2 \alpha_j \cos \alpha_j) \tag{28}$$

C_f is the skin friction drag, α_j is angle of attack between the inclined cable element (cylinder) and the wind and C_{Dbasic} is the drag coefficient of the element if α_j is equal to zero. The angle of attack for a cable element is the angle between its orientation and the relative flow vector. The relative velocity of the element ($\mathbf{v_{Rj}}$) is the difference between the inertial velocity of the element ($\mathbf{v_j}$) and the wind vector acting on the element ($\mathbf{w_j}$):

$$\mathbf{v_{Rj}} = \mathbf{v_j} - \mathbf{w_j} \tag{29}$$

The angle of attack of each element is given by the geometric definition of vector dot product:

$$\cos \alpha_j = \frac{\mathbf{E_j} \cdot \mathbf{v_{Rj}}}{|\mathbf{E_j}||\mathbf{v_{Rj}}|} \tag{30}$$

The following unit vectors with respect to the inertial frame are obtained for the drag and lift force on each segment of the cable:

$$\mathbf{e_{Dj}} = -\frac{\mathbf{v_{Rj}}}{|\mathbf{v_{Rj}}|}$$

$$\mathbf{e_{Lj}} = -\frac{(\mathbf{v_{Rj}} \times \mathbf{E_j}) \times \mathbf{v_{Rj}}}{|(\mathbf{v_{Rj}} \times \mathbf{E_j}) \times \mathbf{v_{Rj}}|}$$

The detailed derivation and assumptions related to these forces can be found in Ref. 1. Note that all the aerodynamic forces are defined using the velocity relative to airmass.

D. Endbody Model

The towed body will be modelled as a small sphere for simplicity. This means that the model will include aerodynamic drag forces for the towed body, but that no aerodynamic lift is generated. The forces due to the towed body will simply be added to the forces acting on the bottom cable point mass. We assume:

$$\mathbf{F_{D_B}} = \frac{1}{2}\rho_a \left|\mathbf{v_{R1}}\right|^2 C_{D_B} \pi r_B^2 \mathbf{e_{D1}} \tag{31}$$

E. System properties

For the purposes of numerical analysis, reasonable values for a medium sized UAV-towed system and environment were selected and these are summarized in Table 1. The choice of bank angle requires a more detailed explanation. The achievable performance for the circularly towed system is very closely tied to the maximum bank angle of the UAV. For a UAV designed particularly with circular towing in mind a bank angle in the range 50 - 70 degrees is conceivable. The target bank angle will be 50 degrees, but in case of upsets, winds and disturbances, up to 70 degrees will be allowed in order to stay on the target path.

III. Guidance and Control Model

The primary objective of tracking control is to derive a means to obtain suitable control input such that the UAV position vector ($\mathbf{p_{UAV}}$) can track a desired path ($\mathbf{p_{UAV_d}}$). The inertial tracking error ($\mathbf{e}$) is defined as:

$$\mathbf{e} = \mathbf{p_{UAV}} - \mathbf{p_{UAV_d}} \tag{32}$$

Defining the control inputs as $(\alpha, T_{UAV}, -\sin\phi)$ we can rewrite the dynamic equations of the UAV as:

$$\begin{bmatrix} \dot{\gamma} \\ \dot{V}_{UAV} \\ \dot{\psi} \end{bmatrix} = \begin{bmatrix} -\frac{g\cos\gamma}{V_{UAV}} + \frac{F_{Cb_3}\sin\phi - F_{Cb_2}\cos\phi}{MV_{UAV}} \\ -g\sin\gamma - \frac{D}{M} + \frac{F_{Cb_1}}{M} \\ \frac{-F_{Cb_3}\sin\phi - F_{Cb_2}\cos\phi}{MV_{UAV}\cos\gamma} \end{bmatrix} + \begin{bmatrix} \frac{\rho_a V_{UAV} C_{L_\alpha} S\cos\phi}{2M} & 0 & 0 \\ 0 & \frac{1}{M} & 0 \\ 0 & 0 & \frac{\rho_a V_{UAV} C_{L_\alpha} S}{2M\cos\gamma} \end{bmatrix} \begin{bmatrix} \alpha \\ T_{UAV} \\ -\sin\phi \end{bmatrix}$$

$$\equiv \mathbf{F} + \mathbf{G}\mathbf{u} \tag{33}$$

In order to achieve robust path control for the strongly nonlinear UAV towed system in the presence of all the uncertainties tied to the UAV model, the towcable dynamics as well as the uncertainties associated with wind prediction and compensation, a sliding mode controller has been chosen.

A. UAV Orbit Characteristics

In the absence of winds, the optimal UAV path is a circular constant altitude orbit where the desired orbit radius and speed are functions of key properties of the towing UAV, the towcable and the towed object, and where the towed object can be stabilized in a circular orbit of much smaller radius offset by most of the towline length directly below the towing UAV.

However, the nice steady-state symmetry of the towing configuration disappears in the presence of even fairly light winds. Due to the aerodynamic forces acting on the towed system, the adjusted path for the towed object is downwind of the orbit formed by the UAV. The lateral offset causes the towline tension to vary over the course of an orbit, resulting in vertical "yoyo" oscillations of the towed object with a frequency that matches the orbit frequency. Additionally, when the UAV is subjected to winds, the UAV airspeed is no longer equal to the UAV groundspeed. Thus the desired UAV airspeed for path planning ($\mathbf{V_{Path}}$) is the difference between the speed of the UAV relative to a point on the ground ($\mathbf{V_{GP}}$) and the windspeed ($\mathbf{V_W}$):

$$\mathbf{V_{Path}} = \mathbf{V_{GP}} - \mathbf{V_W} \tag{34}$$

For the setup in Fig 1 we have:

$$\mathbf{V_{Path}} = (-V_{GP}\sin\theta - V_W)\vec{I} + V_{GP}\cos\theta\vec{J} \tag{35}$$

Table 1. Properties for numerical analysis

Parameter	Value	Notes
	UAV MODEL	
ρ_a	1.225 kg/m^3	ISA sea-level value. Ignore altitude dependence
M	15 kg	Reasonable value for a mid-sized UAV Uncertainty +/- 2 kg
C_{L_α}	1.3	Reasonable value for a mid-sized UAV Uncertainty +/- 0.2
α_0	0.0	Assumed for simplicity
S	0.79	Reasonable guess
C_{D_p}	0.02	Reasonable guess Uncertainty +/- 0.01
e	0.9	Reasonable guess
AR	10	Reasonable guess
ϕ_{tgt} ϕ_{max}	50 deg 70 deg	A reasonable guess An optimistic guess
$V_{UAV_{min}}$	15 m/s	A reasonable guess
$V_{UAV_{max}}$	50 m/s	A reasonable guess
n_{UAV}	25 kg/m^2	A reasonable guess
	CABLE-BODY	
$C_{D_{basic}}$	1.1	Data from Figure 18 in Ref. 9
C_f	0.02	Data from Figure 18 in Ref. 9
C_{D_B}	0.47	Data from Figure 10 in Ref. 9
σ_{UT}	3000 MPa	Honeywell Spectra 1000 Fiber http://www.matweb.com
E	172 GPa	Same as above
ρ_c	970 kg/m^2	Same as above
m_B	2 kg	A reasonable guess
d	0.002 m	A reasonable guess
T_N	37.5 N	Nominal cable tension at towpoint Uncertainty +/- 10 N

Refer to Fig 3 for an illustration of the terminology. At slow speeds it is desirable to control the airspeed in order to maintain a safe margin to the stall speed. An expression for the desired angular velocity in order to maintain constant airspeed in the presence of winds can be derived from equation (35). By taking the magnitude of both sides and simplifying, we obtain the following quadratic equation:

$$V_{GP}^2 + (2V_W \sin\theta)V_{GP} + (V_W^2 - V_{Path}^2) = 0 \tag{36}$$

By inserting $V_{GP} = \dot{\theta} R_{UAV}$ and allowing an arbitrary wind direction (θ_0) we obtain:

$$\dot{\theta} = -\frac{V_w \sin(\theta - \theta_0)}{R_{UAV}} + \frac{\sqrt{V_w^2 \sin^2(\theta - \theta_0) + V_{Path}^2 - V_w^2}}{R_{UAV}} \tag{37}$$

B. Nominal Path derived for No Wind Scenario

As mentioned in the previous section a nominal UAV path can be produced for a particular towed system where an optimized orbit speed and bank angle vary as a function of the weight of the UAV and the length of towline. Both the UAV weight and the towline length are assumed to be fixed values for the purpose of this study. The optimized achievable path considers the relevant system constraints as described in Ref.1 including minimum and maximum speeds of the UAV ($Vmin$ and $Vmax$), minimum cable diameter to not exceed the breaking strength of the cable, minimum achievable UAV orbit radius and maximum allowable bank angle. For now, the UAV is assumed to have unlimited thrust. Fig 4 taken from Ref.1 illustrates the achievable nominal towing configurations for a range of airspeeds for a 600 meter long towcable based on the system parameters defined in Table I. Note that $Rmin(LL)$ and $Rmin(V)$ represents the load-limited UAV turnradius and the airspeed limited UAV turnradius respectively. The optimized towing configuration is summarized in Table 2. The optimized path parameters are inserted into the equation for angular velocity for a circular path that was derived in the previous section to obtain the desired nominal trajectory.

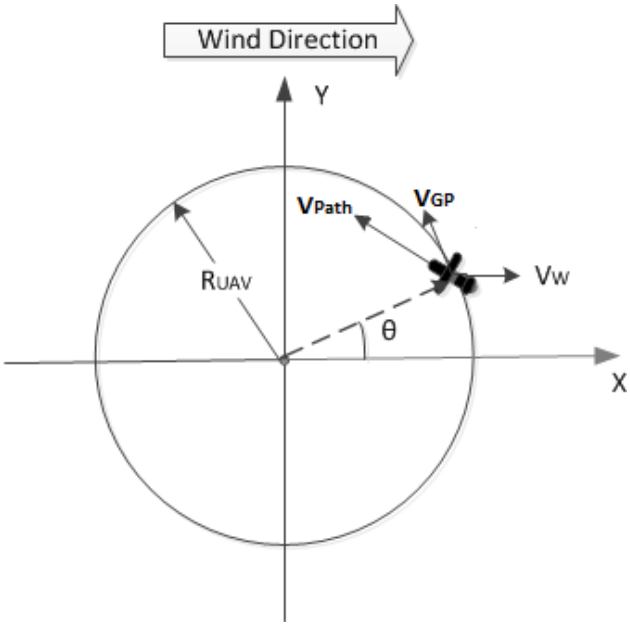

Figure 3. UAV Circular Orbit in Wind

Table 2. Optimized Towing Configuration[1]

UAV Speed	UAV Orbit Radius (UAV Bank Angle)	UAV Height	(Endbody Radius)
20.4 m/s	35.5 m (50 deg)	591.4 m	1.02 m

C. Path Control Strategy considering Winds

From a path control point of view it is desirable to counter the effect of the wind on the system with some type of simple compensation maneuver, hence allowing continued use of the optimized steady-state orbit solution. Different methods have been considered in past studies:

- Use of a high speed cable reel to reel out/in as the aircraft orbits up/down wind[6]
- Fly a non-constant altitude orbit. i.e. incline the orbit[4,6]
- Adjust bank angle based on aircraft heading relative to wind[2]

A key control scheme limitation is that a normal instant feedback strategy cannot be employed. Previous work has revealed that it is necessary to allow up to two orbit periods after a control adjustment for the transients to settle down and the effect of the update to be evaluated.[2] Of the three options listed above, the

second alternative appear to be the most promising for a UAV towed system. The use of a high-speed cable reel is deemed to be too complex and heavy for use onboard the UAV. Adjusting bank angle based on aircraft heading is not expected to give any better performance than the altitude tilted path, but may be required if the tilted path is difficult to implement and maintain (such as for the manned TACAMO missions). Flying a tilted path should be fairly straight forward with a UAV equipped with a standard waypoint-based autopilot. When wind shifts the center of the towed endbody orbit down from the UAV towing orbit, the cable tension can be stabilized by forcing the UAV to descend when flying against the wind and forcing it to climb when flying with the wind. Refer to Fig 5 for an illustration of this concept. As a fairly simple implementation is desired, the descent and ascent is performed at a constant negative and positive vertical rate respectively.

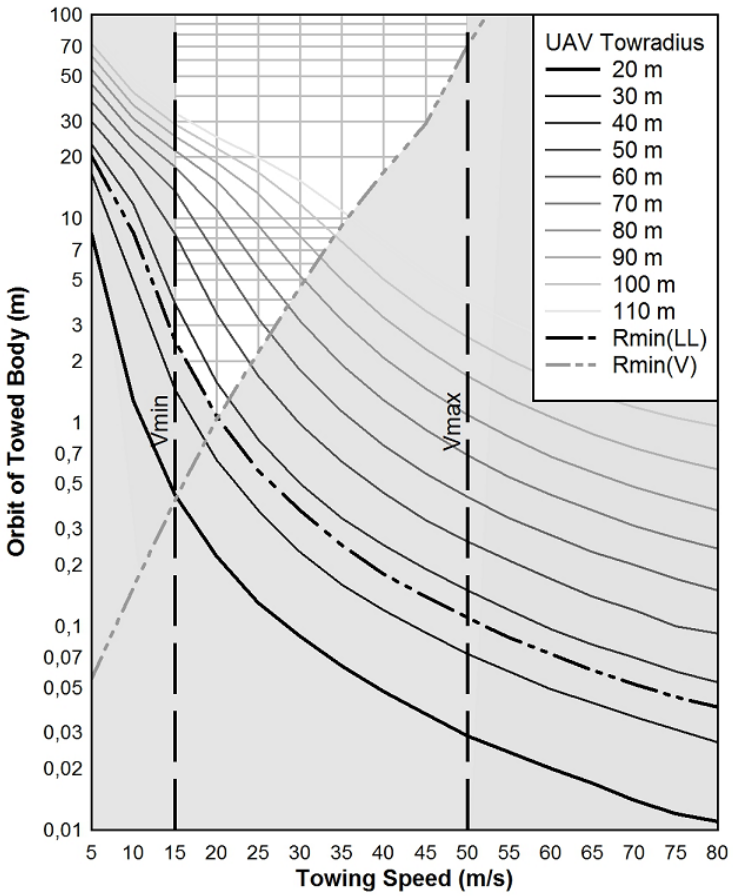

Figure 4. Achievable Towed System Performance with 600 meter Towcable (From Ref. 1).

In order to estimate the required orbit tilt angle, several approaches appear feasable, much dependent on the instrumentation available onboard the UAV and/or the towed endbody. The ultimate goal is to measure/predict the magnitude of the mean vertical oscillations of the endbody. The oscillations can then be cancelled out by setting the maximum deviation from the nominal UAV altitude (ΔH_{max}) equal to the mean vertical endbody deviation (i.e. to half the peak-to-peak oscillation magnitude). The tilt angle (γ_{tilt}) can then be computed from the UAV towing radius (R_{TP}) and (ΔH_{max}) :

$$\gamma_{tilt} = \sin^{-1}\left(\frac{\Delta H_{max}}{R_{TP}}\right) \tag{38}$$

Additional compensations can be made based on measured enduring tension oscillations. The X and Y coordinates of the aircraft trajectory are found using the same strategy as for a constant altitude circular orbit. A slightly more sophisticated method may utimately be required to ensure that the modified path considers the UAV performance constraints.

D. Sliding Mode Controller

Sliding Mode Control provides robust control under the matching condition, i.e. for uncertain terms that enter the state equations at the same point as the control input. It provides a systematic method that guarantees stability and consistent performance as long as the system uncertainties stay within a certain bound.[10,11] The main challenges tied to this method is that an ideal sliding mode controller performs so well through the means of high controller activity which may excite unmodelled dynamics. A number of methods to address this problem, typically referred to as chattering, exist in the litterature. Some of these have been implemented and tested, while additional work may be required following more extensive simulation and/or flight testing.

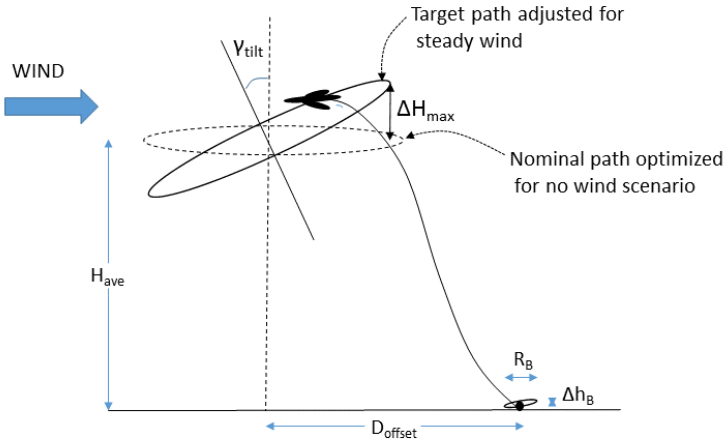

Figure 5. Altitude-tilted Circular Towing in Winds

A sliding mode control strategy consists of two different parts, each filling a specific purpose. The first part consists of the design of a sliding surface (manifold) such that once the system is sliding along the manifold the motion satisfies the design specifications. In the *Sliding Phase* the states should remain on the surface and the surface should be designed such that the states tends to the origin. The second part involves design of a controller that makes the sliding surface attractive to the system states, i.e. that drives the system trajectories to the sliding manifold in finite time in what is referred to as the *Reaching Phase* or *Hitting Phase*.

For the UAV path control problem, we start by rewriting the equations of motion in normal form. We first note that $\dot{\mathbf{V}}_\mathbf{R}$ can be expressed as:

$$\dot{\mathbf{V}}_\mathbf{R} = \mathbf{M}\left[\dot{\gamma}, \dot{V}_{UAV}, \dot{\psi}\right]^T = \mathbf{M}\left(\mathbf{F} + \mathbf{G}\mathbf{u}\right) \tag{39}$$

where $\mathbf{M}$ is given by:

$$\mathbf{M} = \begin{bmatrix} V_{UAV}\mathrm{s}\psi\mathrm{s}\gamma & -\mathrm{c}\gamma\mathrm{s}\psi & -V_{UAV}\mathrm{c}\psi\mathrm{c}\gamma \\ -V_{UAV}\mathrm{s}\gamma\mathrm{c}\psi & \mathrm{c}\gamma\mathrm{c}\psi & -V_{UAV}\mathrm{c}\gamma\mathrm{s}\psi \\ V_{UAV}\mathrm{c}\gamma & \mathrm{s}\gamma & 0 \end{bmatrix} \tag{40}$$

We can formulate the system equations in terms of the tracking error $\mathbf{e}$. Since the relative degree of the system is 2, we select:

$$\dot{\mathbf{e}}_\mathbf{1} = \mathbf{e_2} = \dot{\mathbf{p}}_\mathbf{UAV} - \dot{\mathbf{p}}_{\mathbf{UAV_d}} \tag{41}$$

$$\dot{\mathbf{e}}_\mathbf{2} = \mathbf{M}(\mathbf{F} + \mathbf{G}\mathbf{u}) - \ddot{\mathbf{p}}_\mathbf{UAV} \tag{42}$$

Next, we will select a sliding surface in the state-space that specifies the desired error dynamics (rather than controlling the system states directly). Hence the tracking problem is reduced to a stabilizing problem. We choose the following PID sliding surface:

$$\mathbf{s} = \mathbf{e_2} + \mathbf{a_1}\mathbf{e_1} + \mathbf{a_2}\int_\mathbf{0}^\mathbf{t} \mathbf{e_1}\mathbf{dt} \tag{43}$$

Note that we can choose the appropriate dynamics for the sliding motion from second order system response theory where the goal is to drive the trajectory to $\mathbf{s} = \mathbf{0}$ and maintain it there. By taking $\mathbf{a_i}$ as a diagonal, positive definite matrix we have that $\mathbf{e_1} \to 0$ as $t \to \infty$. The rate of change of the sliding variable $\mathbf{s}$ is given by:

$$\dot{\mathbf{s}} = \mathbf{M}\mathbf{F} + \mathbf{M}\mathbf{G}\mathbf{u} - \ddot{\mathbf{p}}_{\mathbf{UAV_d}} + \mathbf{a_1}\mathbf{e_2} + \mathbf{a_2}\mathbf{e_1} \tag{44}$$

While in the sliding phase, the required control input reduces to an equivalent control $\mathbf{u_{eq}}$ that can be obtained by combining the UAV dynamic equations with $\dot{\mathbf{s}} = \mathbf{0}$. Hence, a good approximation of a continuous control law to remain on the sliding surface is:

$$\hat{\mathbf{u}}_{\mathbf{eq}} = (\mathbf{M}\hat{\mathbf{G}})^{-1}(\ddot{\mathbf{p}}_{\mathbf{UAV_d}} - \mathbf{M}\hat{\mathbf{F}} - \mathbf{a_1}\mathbf{e_2} - \mathbf{a_2}\mathbf{e_1}) \tag{45}$$

Above, $\hat{\mathbf{G}}$ and $\hat{\mathbf{F}}$ are based on the nominal values of the system parameters. It is obvious that we need an additional controller term to reach the sliding surface ($\mathbf{s} = \mathbf{0}$) in finite time and to remain there in the presence of modelling inaccuracies (i.e. to achieve the desired robustness). A switching controller term $\mathbf{v}$ must be designed to drive the trajectories onto (or very near) the sliding surface. A key aspect to consider is to minimize the gain and hence amplitude of the switch in order to minimize chattering. The procedure followed to derive the switching controller is based on Ref. 12.

The switching control term is taken as:

$$\mathbf{v} = (\mathbf{M}\hat{\mathbf{G}})^{-\mathbf{1}}\mathbf{k_d}\text{sign}(\mathbf{s}) \tag{46}$$

where $\mathbf{k_d}$ is a diagonal matrix with the elements of a three dimensional vector $\mathbf{k}$, on the diagonals. In order to satisfy the sliding condition,[11] $\mathbf{k}$ must be chosen such that the following holds:

$$\frac{1}{2}\frac{d}{dt}s_i^2 = s_i\dot{s}_i \leq -\eta_i|s_i| \tag{47}$$

The complete control input is determined by subtracting the switching/robust control term $\mathbf{v}$ from the estimated equivalent control term $\hat{\mathbf{u}}_{\mathbf{eq}}$:

$$\mathbf{u} = \hat{\mathbf{u}}_{\mathbf{eq}} - \mathbf{v} \tag{48}$$

The required switching magnitude is based on the upper bound of the perturbation relative to $\hat{\mathbf{u}}_{\mathbf{eq}}$ which can be calculated from the assumed uncertainties tied to the UAV mass, aerodynamic coefficients and towcable tension as summarized in Table I. The bound on the vector $\mathbf{MF}$ is given by:

$$\left|\mathbf{M}\hat{\mathbf{F}} - \mathbf{MF}\right| \leq \mathbf{F_{max}} \tag{49}$$

And the bound on $\mathbf{G}$ is given by:

$$\mathbf{G} = (\mathbf{I_3} + \mathbf{\Delta})\hat{\mathbf{G}}, \quad \text{where } |\mathbf{\Delta}| \leq \mathbf{D_B} \tag{50}$$

Inserting equations (46), (48) and (61) into (60) gives:

$$\dot{\mathbf{s}} = \mathbf{G}\hat{\mathbf{G}}^{-\mathbf{1}}\left(\ddot{\mathbf{p}}_{\mathbf{UAV_d}} - \mathbf{M}\hat{\mathbf{F}} - \mathbf{a_1}\dot{\mathbf{e}}_{\mathbf{1}} - \mathbf{a_2}\mathbf{e_1} - \mathbf{k_d}\text{sign}(\mathbf{s})\right) + \mathbf{MF} - \ddot{\mathbf{p}}_{\mathbf{UAV_d}} + \mathbf{a_1}\dot{\mathbf{e}}_{\mathbf{1}} + \mathbf{a_2}\mathbf{e_1} \tag{51}$$

Inserting the bound on the input matrix given in (50) we get:

$$\dot{\mathbf{s}} = (\mathbf{MF} - \mathbf{M}\hat{\mathbf{F}}) - \mathbf{k_d}\text{sign}(\mathbf{s}) - \mathbf{\Delta}\mathbf{k_d}\text{sign}(\mathbf{s}) + \mathbf{\Delta}\mathbf{a} \tag{52}$$

where

$$\mathbf{a} = \ddot{\mathbf{p}}_{\mathbf{UAV_d}} - \mathbf{M}\hat{\mathbf{F}} - \mathbf{a_1}\dot{\mathbf{e}}_{\mathbf{1}} - \mathbf{a_2}\mathbf{e_1} \tag{53}$$

We continue to design $\mathbf{v}$ to form a control law such that each $\frac{1}{2}s_i^2$ is a Lyapunov-like function that ensures the trajectory is driven to the $\mathbf{s} = \mathbf{0}$ manifold. We have:

$$s_i\dot{s}_i = s_i\left[(MF)_i - (M\hat{F})_i - \sum_{j=1}^{3}(\Delta_{ij}k_j\text{sign}(s_j) + \Delta_{ij}a_j)\right] - k_i\text{sign}(s_i)s_i \tag{54}$$

The sliding condition is satisfied if $\mathbf{k}$ is chosen such that $s_i\dot{s}_i$ is smaller than $-\eta|s_i|$. By substituting in the upper bound on the model uncertainties (49) and (50), we obtain:

$$s_i\dot{s}_i \leq \left[F_{max_i} + \sum_{j=1}^{3}(D_{B_{ij}}k_j + D_{B_{ij}}|a_j|)\right]|s_i| - k_i|s_i| \leq -\eta_i|s_i| \tag{55}$$

Simplifying gives:

$$k_i - \sum_{j=1}^{3} D_{B_{ij}} k_j \geq F_{max_i} + \sum_{j=1}^{3} D_{B_{ij}} |a_j| + \eta_i \tag{56}$$

If we rewrite the equation in vector form we get:

$$(\mathbf{I_3} - \mathbf{D_B})\mathbf{k} \geq \mathbf{F_{max}} + \boldsymbol{\eta} + \mathbf{D_B} \left| -\mathbf{M}\hat{\mathbf{F}} + \ddot{\mathbf{p}}_{\mathbf{UAV_d}} - \mathbf{a_1}\dot{\mathbf{e}}_\mathbf{1} - \mathbf{a_2}\mathbf{e_1} \right| \tag{57}$$

Finally, we can choose a $\mathbf{k}$ to satisfy this constraint:

$$\mathbf{k} = (\mathbf{I_3} - \mathbf{D_B})^{-1} \left[\mathbf{F_{max}} + \boldsymbol{\eta}\right] + \mathbf{D_B} \left[-\mathbf{M}\hat{\mathbf{F}} + \ddot{\mathbf{p}}_{\mathbf{UAV_d}} - \mathbf{a_1}\dot{\mathbf{e}}_\mathbf{1} - \mathbf{a_2}\mathbf{e_1} \right] \tag{58}$$

As an additional measure to reduce chattering, we will replace the signum function with a high-slope saturation function:

$$\text{sat}\left(\frac{s_i}{b_{t_i}}\right) = \begin{cases} \frac{s_i}{b_{t_i}} & \text{if } |s_i| \leq b_{t_i} \\ \text{sign}(s_i) & \text{if } |s_i| > b_{t_i} \end{cases} \tag{59}$$

The boundary layer thickness (b_t) can be adjusted such that tracking accuracy can be traded off to remove undesired high control activity.

The controller specified above was implemented and tested in a simulation. However, time constraints prevented the generation of all the data in the next section using the proper sliding mode controller. A modified version of the equivalent controller $\hat{u}_{eqm}$ was used to collect the towing performance data. It was derived by adding a term that would drive the controller to $\mathbf{s} = \mathbf{0}$:

$$\begin{aligned} \dot{\mathbf{s}} + \mathbf{a_3}\mathbf{s} = \ddot{\mathbf{p}}_{\mathbf{UAV_d}} - \mathbf{M}\left(\mathbf{F} + \mathbf{G}\mathbf{u}\right) + (\mathbf{a_1} + \mathbf{a_3})\mathbf{e_2} \\ + (\mathbf{a_1}\mathbf{a_3} + \mathbf{a_2})\mathbf{e_1} + \mathbf{a_2}\mathbf{a_3}\int_{\mathbf{0}}^{\mathbf{t}} \mathbf{e_1}\mathbf{dt} = 0 \end{aligned} \tag{60}$$

Thus the following controller was used:

$$\begin{aligned} \hat{\mathbf{u}}_{\mathbf{eqm}} = (\mathbf{M}\hat{\mathbf{G}})^{-1}(\ddot{\mathbf{p}}_{\mathbf{UAV_d}} - \mathbf{M}\hat{\mathbf{F}} - \mathbf{a_1}\mathbf{e_2} - \mathbf{a_2}\mathbf{e_1} \\ + (\mathbf{a_1}\mathbf{a_3} + \mathbf{a_2})\mathbf{e_1} + \mathbf{a_2}\mathbf{a_3}\int_{\mathbf{0}}^{\mathbf{t}} \mathbf{e_1}\mathbf{dt}) \end{aligned} \tag{61}$$

Careful testing of the robustness we achieve using the SMC will be the subject of future work.

IV. Simulator Results

This section presents the results of the simulated towed system described in the previous sections. The results have been generated using the controller settings summarized in Table 3. The optimized nominal

Table 3. Sliding Mode Controller Settings

Parameter	u_α	u_T	u_ϕ
a_1	3.0	3.0	3.0
a_2	1.0	1.0	1.0
a_3	25.0	25.0	25.0

towing scenario where the UAV is towing the cable in still air (no wind or disturbances), is shown in Fig 6. The "UAV Path Tracking" compares the target optimal path and the actual UAV orbit, showing that the controller tracks the desired path well. This tracking performance is representative for all the cases discussed in this section, unless otherwise noted. We can conclude that the towed endbody orbits the inertial Z axis

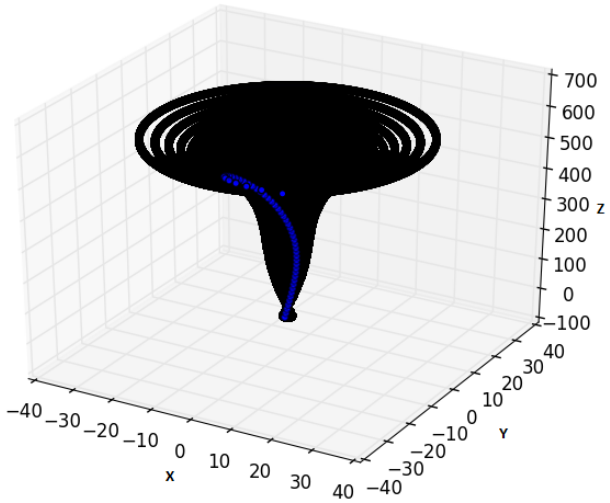

(a) SS Surface formed by Towcable

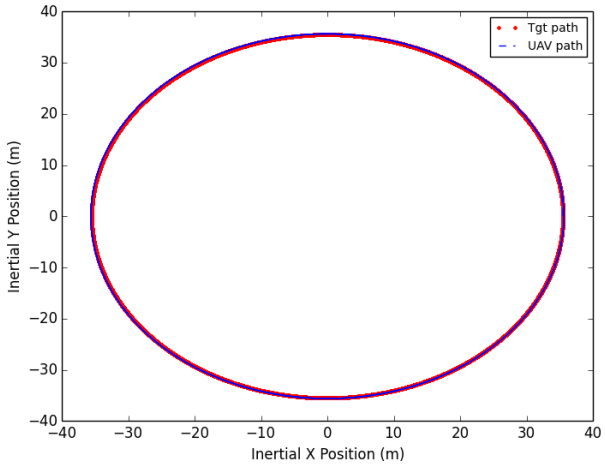

(b) UAV Path Tracking

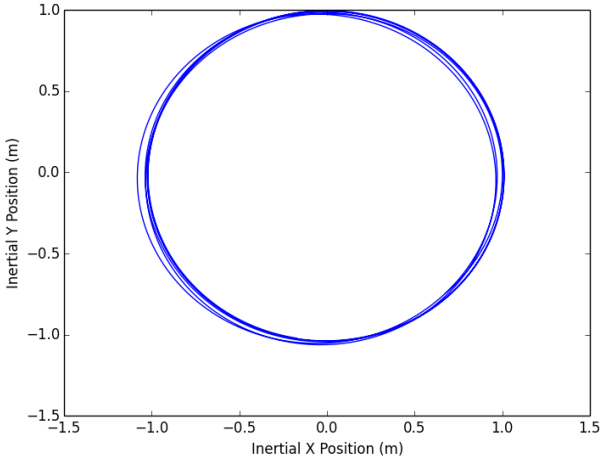

(c) SS Endbody Path

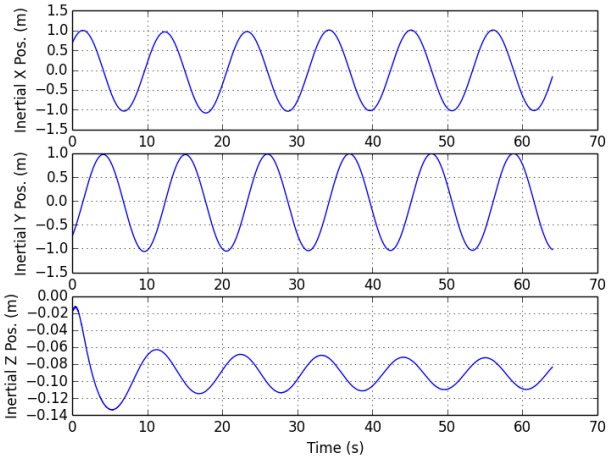

(d) Endbody Inertial Positions

Figure 6. Case1. Nominal Circular Towing (No wind)

with a radius of about 1 meter. The endbody orbit speed is about 0.6 m/s. Also, the vertical motion of the endbody is on the order of 0.04 meter.

These results indicate that the circular towing method using a fixed-wing UAV is promising for high precision endbody operations such as object placement and pickup. However, real operating conditions will never be this perfect (no wind or disturbances), and certainly not so in the Arctic. Hence, the perfomance of the system when subjected to steady winds will be considered next. A steady wind of 3 m/s and 6 m/s is selected for closer study. Fig 7 show the equivalent performance for the 3 m/s case if the UAV is controlled to constant airspeed and no attempt is made to compensate for the wind. The cable is initiated at the no-wind equilibrium condition, and the wind is ramped from 0 to 3 m/s at the start of the simulation. We

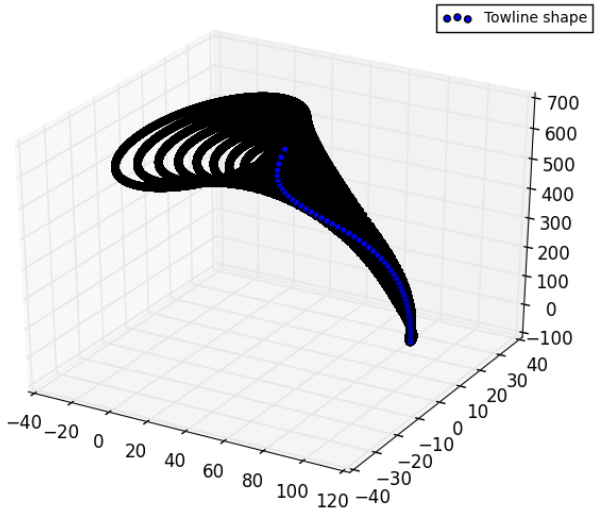

(a) SS Surface formed by Towcable

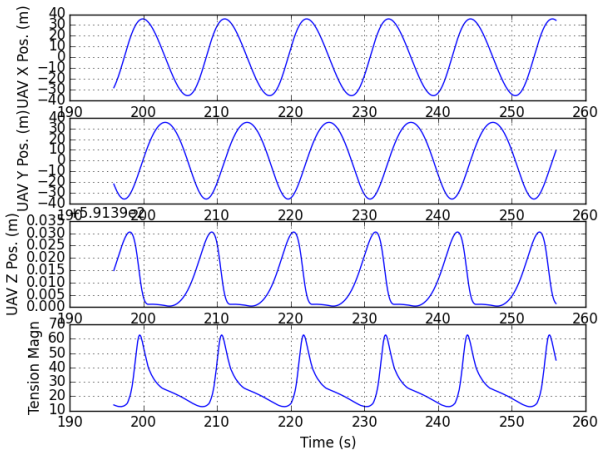

(b) UAV Path Tracking

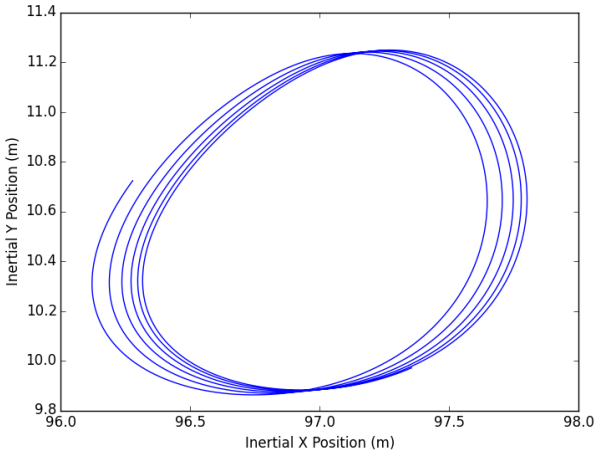

(c) SS Endbody Path

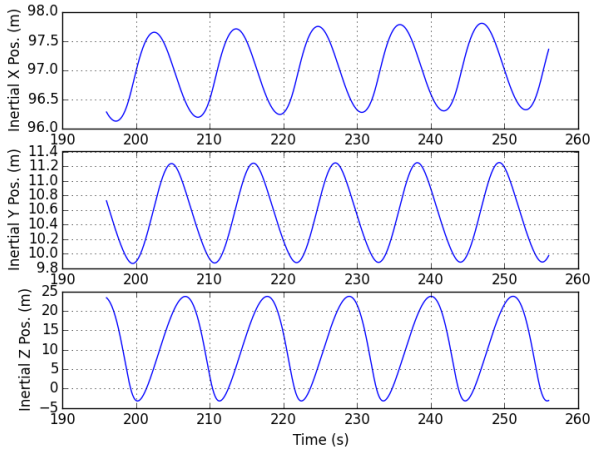

(d) Endbody Inertial Positions

Figure 7. Case2. Circular Towing- 3 m/s wind

note that it takes over 4 minutes after the upset for the cable to (almost) stabilize. In order to illustrate the new "steady-state surface" formed by the orbiting cable, Fig 7a includes data from the final orbit made by the UAV only. As expected, the aerodynamic forces acting on the cable in the presence of the wind forces the cable to stabilize downwind from the towing UAV. The towed endbody is now shifted over 90 meters downwind and also slightly to the North (10 meters) of the UAV orbit center. The shift of the endmass orbit centre to the North (positive Y- position) is explained by the fact that the UAV spends more time flying upwind (positive Y-position) than downwind (negative Y-position). The horizontal motion is small but the vertical oscillations are now on the order of 26 meters peak-to-peak. A plot showing the motion of the UAV and the cable tension at the top of the towcable is shown in Fig 7b. We see that a maximum tension of 62

N occurs as the UAV is flying directly into the wind, while the minimum tension of 12 N is experienced as the UAV flies directly downwind.

For a 6 m/s wind, the cable is pushed further downwind with even higher vertical oscillations as illustrated in Fig 8. Note that only the last minute of the 3 minute run-time is shown in these figures. At 6 m/s the towing UAV started to have trouble to follow the desired path perfectly. Since the bank angle is limited to a maximum of 70 degrees (the target bank angle is 50 degrees) it gets temporarily pushed off the path on the downwind (high-speed) leg, showing that we are approaching the upper limit of what this configuration of the towed system can sustain while still delivering an acceptable service. At higher winds it will be necessary to select a different optimal steady-state solution (as illustrated in Fig 4), involving a larger UAV towing radius and/or speed resulting in larger motion of the towed endbody.

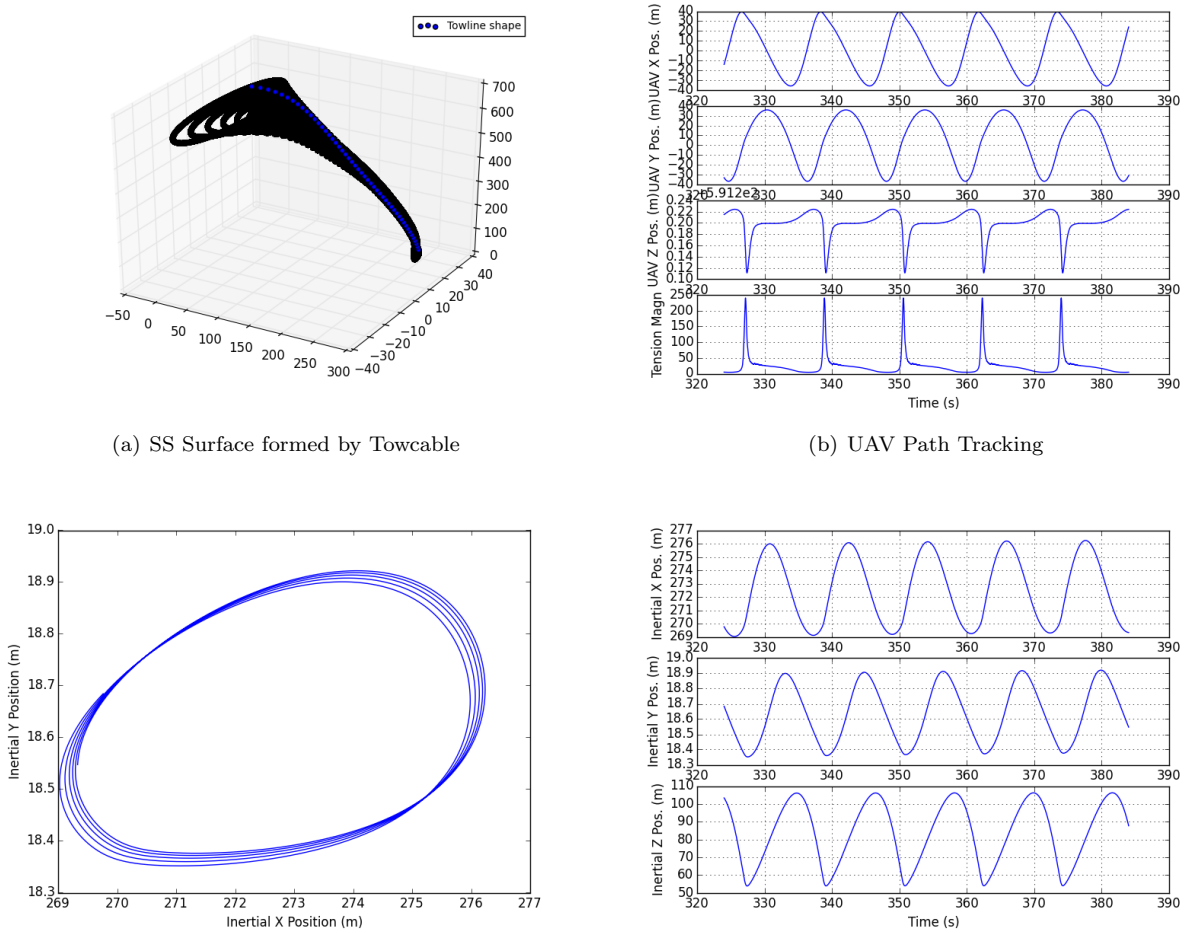

(a) SS Surface formed by Towcable

(b) UAV Path Tracking

(c) SS Endbody Path

(d) Endbody Inertial Positions

Figure 8. Case 3. Circular Towing- 6 m/s wind

In order for the system to be useful for object placement/pickup applications when subjected to winds, it is clearly desireable to reduce the vertical motion of the cable endbody as mush as possible. The altitude-tilted orbit approach described in section III C is adopted. Here ΔH_{max} is taken to be half of the peak-to-peak oscillation magnitude of the endbody, so 13 meters for the 3 m/s wind case. The resulting UAV path is described in Fig 9. The tilting of the orbit has reduced the vertical peak-to-peak motion of the endbody from 26 meters to about 6.5 meters. Data was also collected assuming ΔH_{max} to be 11 meters and 15 meters, but for both cases the endbody peak-to-peak magnitude was slightly worse (about 7.5 meters and 8.5 meters respectively). It does not seem that it is feasible to remove all the vertical oscillations using this technique, which may not be surprising given that the UAV tries to impact the motion of the endbody by means of a long flexible cable. The steady-state orbit of the endbody in the horzontal plane is fairly similar

to that achieved in no wind. The tension magnitude at the top of the cable is more even over the course of an orbit than for the no-tilt case where the tension went from high to low in half a UAV orbit: The tension magnitude is also slightly lower, varying between 5 N and 50 N. This finding supports a strategy where the tension of the towcable can be measured onboard the UAV and serve as an input to UAV path planning and control in order to minimize the endbody motion. The scenarios that were analyzed are summarized in

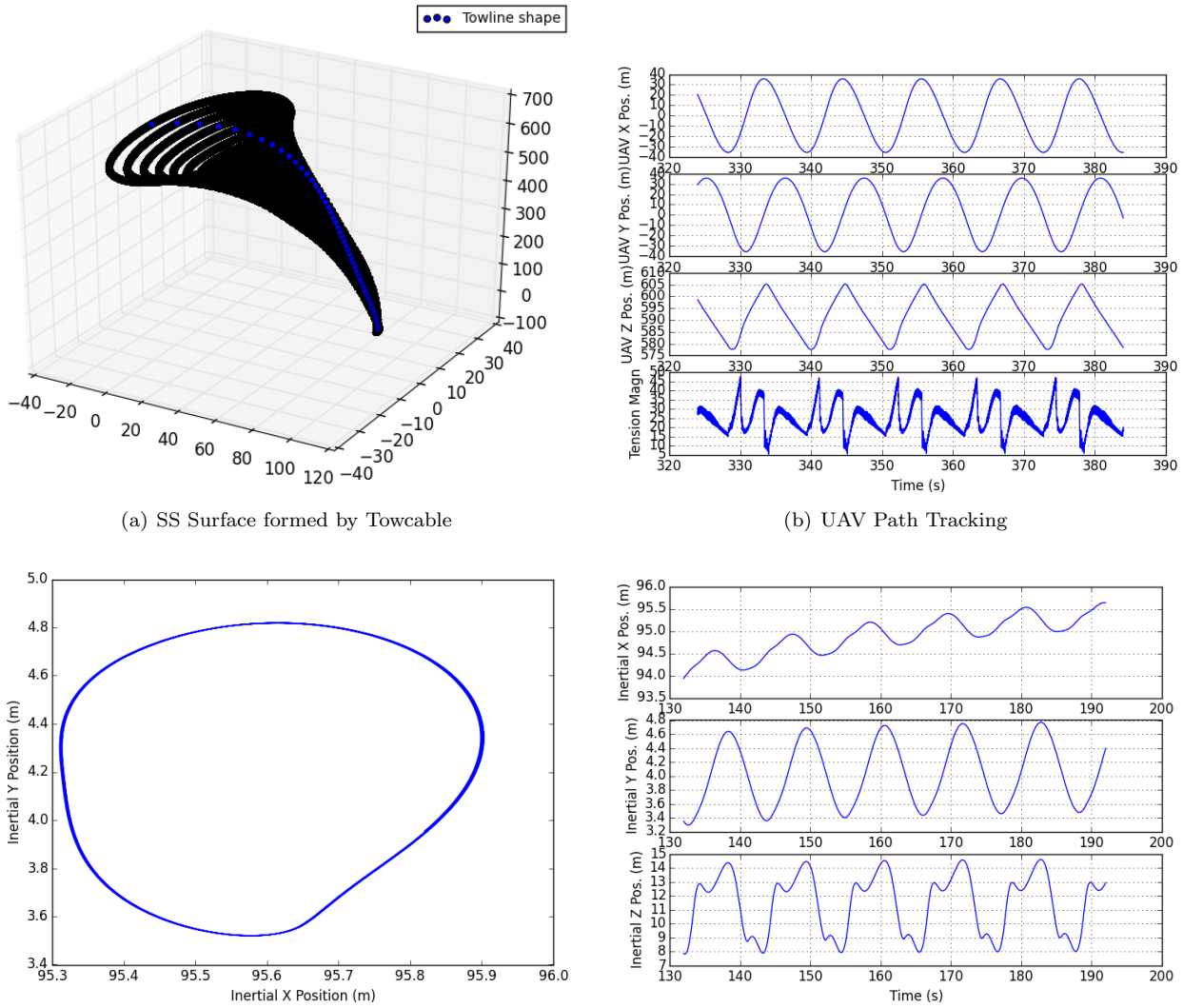

(a) SS Surface formed by Towcable

(b) UAV Path Tracking

(c) SS Endbody Path

(d) Endbody Inertial Positions

Figure 9. Case 4. Circular Towing with Tilted Orbit- 3 m/s wind

Table III. Note that the UAV mean height above ground was 600 meters for all the simulated cases.

Table 4. Summary of simulated cases

Case	V_W	R_{TP}	V_{UAV}	Path Tilt
1	0 m/s	35.5 m	20.4 m/s	No
2	3 m/s	35.5 m	20.4 m/s	No
3	6 m/s	35.5 m	20.4 m/s	No
4	3 m/s	35.5 m	20.4 m/s	Yes

Key performance characteristics for these scenarios are summarized in Table IV.

Table 5. Performance of simulated cases

Case	D_{offset}	Avg R_B	δH_B
1	0 m	$\approx 1.0m$	$\approx 0.04m$
2	$\approx 97m$	$\approx 1.0m$	$\approx 26m$
3	$\approx 272.5m$	$\approx 2.0m$	$\approx 50m$
4	95.6 m	$\approx 1.0m$	$\approx 6.5m$

V. Conclusion

A strategy has been developed for close to optimal path planning for a towing UAV in order to minimize the motion on the towed endbody in the presence of winds. Also, a robust sliding mode controller has been derived in order to provide robust UAV path control. The proposed path planning and control algorithms have been verified in a simulator. It is possible to stabilize the endbody with a relatively small motion when subjected to a moderate breeze, but with a signifincant lateral offset to the towing UAV. In order to perform a pick-up maneuver, means to control the endbody separate from the towing UAV will increase the odds of mission success significantly.

References

[1]Mariann Merz and Tor Arne Johansen *Feasability Study of a Circularly Towed Cable-Body System for UAV Applications*, Accepted for International Conference on Unmanned Aircraft Systems 2016, Arlington, VA, USA, June 7. - 10, 2016.

[2]Robert G. Borst, Glen F. Greisz, and Allen G. Quynn *Fuzzy Logic Control Algorithm for Suppressing E-6A Long Trailing Wire Antenna Wind Shear Induced Oscillations*, AIAA Guidance, Navigation, and Control Conference, Monterey, CA, USA, August 9-11, 1993.

[3]Donald L.J. Brushwood, Anthony P. Olson, and Joseph M. Smyth *The E-6A Orbit Improvement System and its Effect Upon LTWA Verticality*, Guidance, Navigation, and Control Conference and Exhibit, Boston, MA, USA, 1998.

[4]James G.R. Hansen, Steven A. Crist *Dynamics of Cables Towed from Aircraft*, United States Airforce Academy, Research report 72-8, October 1972.

[5]Richard M. Murray *Trajectory Generation for a Towed Cable System using Differential Flatness*,IFAC Word Congress, San Francisco, July 1996.

[6]Paul Williams *Optimization of Circularly Towed Cable System in Crosswind* Journal or Guidance, Control, and Dynamics, Vol. 33, No. 4, July - August 2010.

[7]M.B. Colton, L. Sun, D.C. Carlson and R.W. Beard *Multi-vehicle dynamics and control for aerial recovery of micro air vehicles* Int. J. Vehicle Autonomous Systems, Vol.9, Nos. 1/2, pp. 78 - 107, 2011.

[8]W. H. Phillips *Stability of a body stabilized by fins and suspended from an airplane* NACA Wartime Report L-28, 1944.

[9]S.F. Hoerner *Fluid Dynamic Drag*, Published by the Author, 1965

[10]Hassan K. Khalil *Nonlinear Systems*, Third Edition, Prentice Hall, Inc., Upper Saddle River, NJ 07459.

[11]J.J.E Slotine, W. Li *Applied Nonlinear Control*, Prentice Hall, New Jersey, 1991.

[12]Barry B. Goeree, Ernest D. Fasse, Martin J.L. Tiernego, Jan F. Broenink *Sliding Mode Control of Spatial Mechanical Systems Decoupling Translation and Rotation*, ASME International Mechanical Engineering Congress and Exposition 1997, November 16-21, 1997, Dallas, TX, USA (pp. pp. 545-554).